Earthquake Engineering, Tenth World Conference © 1992 Balkema, Rotterdam. ISBN 90 5410 060 5

Mechanics of elastomeric seismic isolation bearings

R. Shepherd & L.J. Billings
University of California, Irvine, Calif., USA

ABSTRACT: The availability of advanced computer codes prompted a finite element study of the mechanics of elastomeric bearings under large compression and shear loads in anticipation that hitherto incompletely understood aspects of the behavior of seismic isolator bearings could be clarified. This paper describes one aspect of this investigation. A low shape factor multilayered elastomeric bearing for which experimental results are available was modeled in three dimensions using a general purpose finite element program, MARC K.4 which includes formulation for elastomeric materials. Comparison with earlier analyses in which the bearing was modeled in two dimensions indicates that the three-dimensional simulation provides significantly improved correlation with the experimentally established behavior.

1 INTRODUCTION

The principle of isolating a structural system from ground vibrations has been understood for many years, and numerous successful implementations exist in which bridges or buildings are mounted on resilient bearings. However, it is only in the last twenty years that designers have developed sufficient confidence to incorporate isolation as the primary means of protecting structures from earthquake-generated strong ground motion.

As with many engineering innovations, successful application of the concept was delayed by difficulty in developing reliable and predictable devices which would not only possess the necessary characteristics at the time of construction, but would preserve these properties throughout the expected life of the structure. Greater understanding of the nature of strong seismic ground movements, and the ability to model structural systems using computers, undoubtedly have benefitted the design process, but the most significant recent advances have been prompted by the development of a range of viable isolator devices. These include various combinations of simple rubber blocks, steel torsional and flexural beams, lead extrusion elements and steel plates interlayered with elastomeric materials [Buckle 1990].

One of the most promising of these devices appears to be the laminated steel/elastomer bearing. By sandwiching a series of relatively thin slices of elastomer between horizontal steel shims, a composite block can be formed possessing the desirable properties of large vertical stiffness and large horizontal flexibility.

The design of laminated bearings is still at the stage of progressive refinement. Elementary considerations in typical use necessarily reflect a very conservative approach, as the behavior of these bearings at high strains is imperfectly understood. Current practice in the United States involves verification testing of a proportion, as high as ten percent, of the isolators manufactured for use in a given project. The tested units are then discarded. In Japan, typically each isolator is tested before installation. The objective in both cases is to verify the integrity of the units in the light of the use of a somewhat simplistic design process, and the undoubted difficulty in assuring quality control of the complex production process.

2 FINITE ELEMENT MODELING

The mathematical model widely used to predict the behavior of elastomeric bearings is based on small strain elastic theory. Stress is assumed linear with respect to strain and the vertical stiffness k_v may be expressed as

$$k_v = \frac{P}{\delta} = \frac{E_c A}{n t} \qquad (1)$$

where P is the vertical load, δ the vertical displacement, A the cross sectional area of the bearing, n the number of elastomeric layers, t the thickness of each layer and E_c an equivalent compression modulus of the elastomer.

A similar approach leads to the horizontal stiffness k_h being expressed as

$$k_h = \frac{F}{\Delta} = \frac{G A}{n t} \qquad (2)$$

where F is the horizontal load, Δ the horizontal displacement, and G the shear modulus of the elastomer.

Modifications of these expressions for bearings with many layers have been suggested [Kelly 1990]. Clearly the equations do not reflect the observed nonlinear behavior of the elastomer, do not account for large deflections, nor do they provide any information on the internal stresses and strains within the bearing. If an improved understanding of the actual behavior of multi-layered isolators is to be developed, a more realistic mathematical model is needed.

One approach utilizes finite elements to represent the elastomer and the steel shims. Since elastomeric bearings

experience large deformations and the elastomer behaves nonlinearly, the finite element formulation must include geometric and material nonlinearities. The most significant problem is representing the elastomer and its material properties. It is difficult to determine the material properties experimentally and the analyses are sensitive to the value of input constants.

The number of elements used to represent the continuum can affect the outcome of the analysis. Many elements are needed where the stress concentrations are high, but this may not be known until after the analysis. Adaptive mesh and rezoning techniques based on previous results are justified. Many bearings with large numbers of layers, some with thirty or more laminates, are now being used. In such cases, the total number of elements may well be of the order of several thousand, and the use of a very large capacity computer is necessary.

2.1 *Three Dimensional Analyses*

A low shape factor bearing tested at the University of California, Berkeley [Aiken 1989, Tajirian 1990] was chosen for finite element analyses using MARC Analysis Research Corporation's MARC K.4 code. Pre-processing of the geometry, boundary conditions, loads, and material properties was undertaken using PDA Engineering's PATRAN 2.5. The top plate of the bearing was bolted, therefore the boundary conditions are that the two end plates remain parallel, the base plate remains fixed, and constraints are invoked along the line of symmetry.

8-noded, 3-dimensional, isoparametric, brick elements represented the steel and 9-noded "Herrmann" elements, with 8 corner nodes and one extra pressure node, represented the elastomer for a total of 5184 elements and 9900 nodes. Each rubber layer received 6 elements through its thickness. The results were sensitive to the coarseness of the cover rubber mesh. Three elements in plan were required through the thickness of the cover rubber, otherwise the bearing behaved too stiff both vertically and horizontally. The analysis was run on U.C. Irvine's CONVEX C240.

The rubber is represented in the code using a potential function $W(I_1, I_2)$ studied by James, Green and Simpson [1975] viz:

$$W(I_1,I_2) = C_{10}(I_1 - 3) + C_{01}(I_2 - 3) + C_{11}(I_1 - 3) + C_{20}(I_1 - 3)^2 + C_{30}(I_1 - 3)^3 \quad (3)$$

where I_1, I_2 and I_3 are strain invariants defined by,

$$I_1 = \lambda_1^2 + \lambda_2^2 + \lambda_3^2 \quad (4)$$

$$I_2 = \lambda_1^2\lambda_2^2 + \lambda_2^2\lambda_3^2 + \lambda_3^2\lambda_1^2$$

$$I_3 = \lambda_1^2\lambda_2^2\lambda_3^2$$

and λ_1, λ_2, and λ_3 are the principal extension ratios. The condition of incompressibility requires that,

$$I_3 = \lambda_1^2\lambda_2^2\lambda_3^2 = 1 \quad (5)$$

and hence I_3 is not a function of the strain. Thus, the potential function W can be expressed as a function of I_1 and I_2 [Treloar, 1975].

The MARC code requires the five constants, C_{10}, C_{01}, C_{11}, C_{20}, and C_{30}, as input. The material is then modeled as nonlinear elastic. The problem of assigning values to the constants has been recognized and some unique options have been discussed such as setting C_{01} and C_{11} to zero and assigning values to C_{10}, C_{20}, and C_{30} [Yeoh, 1990]. The difficulty lies in justifying the assigned values. Assistance from the Malaysian Rubber Producers' Research Association (MRPRA) in Hertford, England was sought regarding the above constants. On the basis of advice received, elastomeric materials used in isolation bearings typically exhibit some hysteresis, therefore, it is justifiable to use simplified forms of the potential function W. It was suggested to use the simplest of all options and set $C_{01} = C_{11} = C_{20} = C_{30} = 0.0$, and fit C_{10} from MRPRA's test data. Taking only the first term yields the Neo-Hookean material model,

$$W(I_1) = C_{10}(I_1 - 3) \quad (6)$$

C_{10} was chosen as 60.0 psi from MRPRA and U.C. Berkeley test data and assigned to all elements representing the elastomer. Hence, the elastomer was modeled as linear, elastic and incompressible.

The elements representing steel were given a higher than typical yield stress of 100,000 psi to prevent yielding in the steel shims.

100 psi per increment vertical load was applied in 5 increments for a total compressive load of 500 psi over the shim area or 15,900 lbs (symmetry considerations allowed only half the bearing to be modeled). A horizontal load of 125 lbs per increment was applied on the top plate in the next 75 increments. Increment 80 was the last recorded increment where convergence was achieved. This loading is the full three-dimensional equivalent of 18,750 lbs horizontal force with 31,800 lbs vertical as was applied in the experiment. The loading histories are shown in Figures 1 and 2. There was a slightly nonlinear response of vertical displacement with increasing horizontal displacement.

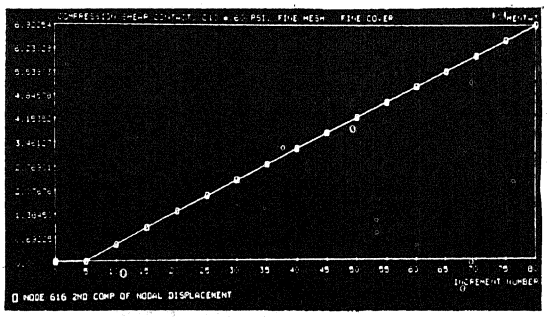

Figure 1. Horizontal displacement vs. load. 125 lbs/ increment shear force applied in increments 6 to 80.

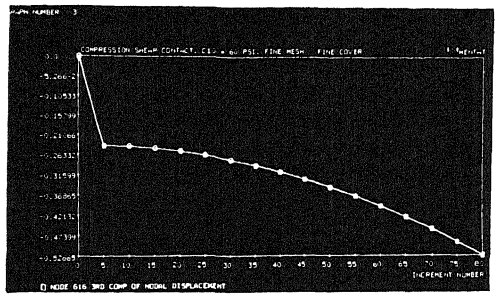

Figure 2. Vertical displacement versus load. 3181 lbs/ increment vertical load applied in increments 1 to 5.

2.2 *Discussion of Results*

The vertical displacement of the bearing under 500 psi compression or 31.8 kips in full 3D is shown in Figure 3. Comparing the F.E.M. displacement of 0.241 inches for the top plate with U.C. Berkeley's experimental results which were a vertical displacement of 0.254 inches at 31.802 kips, showed agreement near 5%.

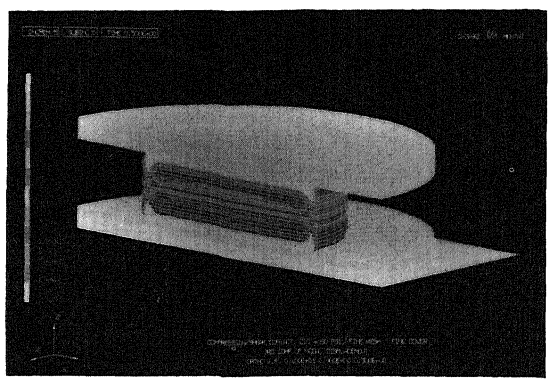

Figure 3. Vertical displacement under 500 psi compression.

The horizontal displacement under 500 psi compression and 5000 lbs shear is shown in Figure 4. Contact between the cover rubber and lower steel plate was allowed for in the analysis and occurs at the lower right and upper left corners of the bearing and continues around the rear. The finite element model's horizontal displacement was 3.73 inches in increment 45 where the equivalent 3D horizontal load was 10000 lbs. The comparable test result was estimated to be 3.85 inches at 10000 lbs shear force from a plot of shear force vs. displacement with 31800 lbs compression. The F.E.M. result was 3% below this value. The hysteretic effects of the rubber were not modeled and hence not expected to be replicated.

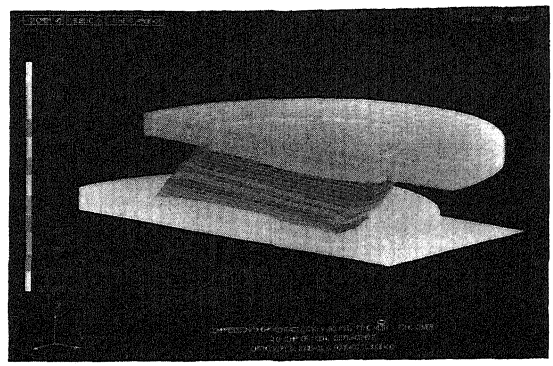

Figure 4. Horizontal displacement under 500 psi compression and equivalent 3D shear load of 10000 lbs.

Figure 5 shows the horizontal displacement under 500 psi compression and equivalent 3D shear load of 18,750 lbs yielding a horizontal displacement of 6.92 inches. The comparable shear test result was estimated to be 6.40 inches at 18750 lbs from a plot of shear force vs. horizontal displacement with 31800 lbs compression. This value is 8% below the F.E.M. result. The experiments showed a stiffening effect above 150% shear strain which was not replicated in this model since the simplest linear elastic model for the elastomer was chosen. Higher order terms in the potential function were set to zero yielding the linear model. Using more constants in the elastomer material formulation would create nonlinear material behavior and the stiffening effect could be replicated, provided the correct values for the constants were input.

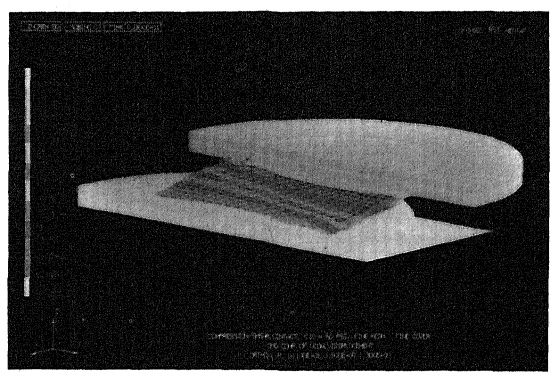

Figure 5. Horizontal displacement under 500 psi compression and equivalent 3D shear load of 18750 lbs.

The maximum Y-component of stress in the steel plate under compression is 7043 psi as shown in Figure 6. This was compared with the value determined using expression (7) for internal stress in the steel shims which does not account for cover rubber [Stanton, 1982]:

$$\sigma_{s,max} = \left[\frac{t_1+t_2}{2t_s}\right]\left[\frac{1.5}{1+1/S^2}\right]\bar{\sigma}_c \qquad (7)$$

where t_1 and t_2 are the thickness of the elastomeric layers on each side of the steel shim, t_s is the thickness of the steel shim, S is the bearing's shape factor, and $\bar{\sigma}_c$ is the compressive stress. Application of this expression to the particular bearing examined yields a maximum stress of 5965 psi which is 15% less than the F.E.M. value.

The shear strain in the elastomer under compression is shown in figure 7. The maximum value of 0.903 occurs at the edge of the rubber-steel interface. Its value was compared with that obtained from the expression for maximum shear strain at the rubber-steel interface, viz:

$$\gamma_c = 6S\bar{\epsilon}_c \qquad (8)$$

where $\bar{\epsilon}_c$ is the compressive strain. The above expression yields a value of $\gamma_c = 1.08$ which is 20% above the F.E.M. value. Based on 2D analysis described later, it is expected that the strain value will converge toward the theoretical value as the F.E.M. model is meshed more finely in the region of maximum shear strain.

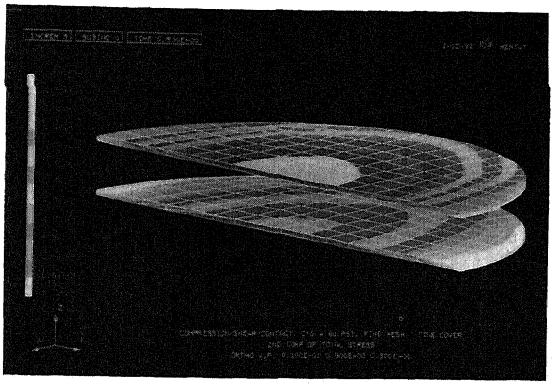

Figure 6. Y-component of stress in the steel under 500 psi compression.

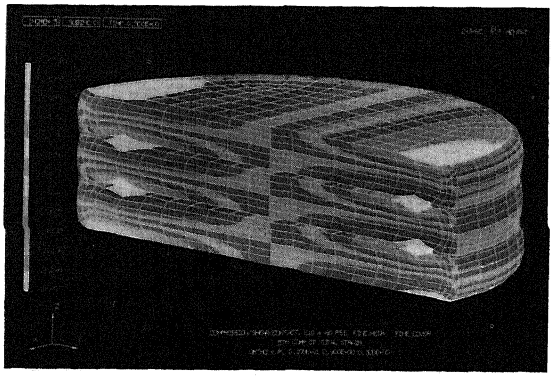

Figure 7. Maximum shear strain in the elastomer under 500 psi compression.

The Von-Mises stress in the steel shims under the equivalent 3D shear load of 10000 lbs, equivalent to nearly 130% shear strain, and 500 psi compression as presented in Figure 8 had a maximum value of 30970 psi. The true yield stress of the steel shims is of the order of 47000 psi, hence the plates are not yielding at this loading. However when the horizontal load reached 20000 lbs at 230% shear strain in the last recorded increment, the Von-Mises stress in the plates was 58750 psi as shown in Figure 9. As stated above, the yield stress in the steel was set at 100,000 psi for this analysis. It is expected that the steel shims will yield under the applied loadings and 47000 psi was reached under 15250 lbs equivalent full 3D shear force or 188% shear strain.

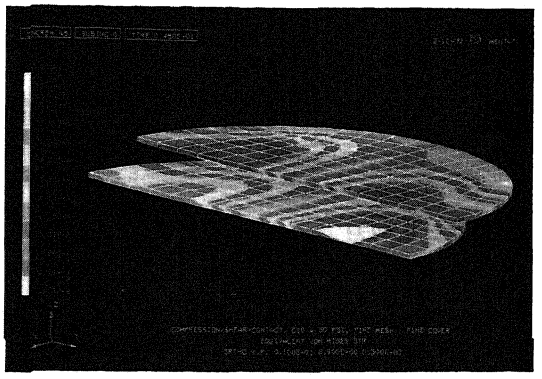

Figure 8. Equivalent Von-Mises stress in the steel shims under 500 psi compression and equivalent 3D shear load of 10000 lbs.

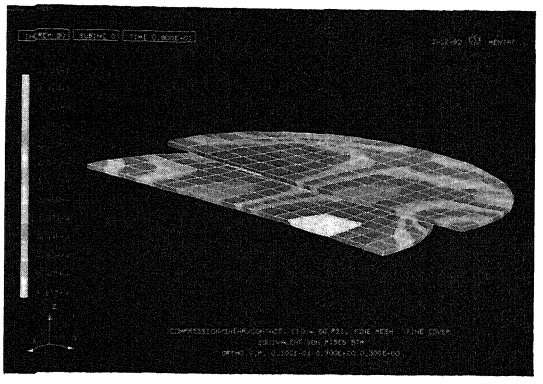

Figure 9. Equivalent Von-Mises stress in steel shims under 500 psi compression and equivalent 3D shear load of 18750 lbs.

Figures 10 and 11 show the Z-component of Cauchy stress in the rubber at increments 45 and 80 representing 125% and 230% shear strains respectively. The cover rubber and some of the internal rubber had gone into 240 psi tension, while the inner elastomer was in compression, taking up vertical load. Also it is noted that the tension value of 240 psi remained nearly constant from increment

45 to 80, but the amount of rubber affected increased. There were large stress concentrations at the rubber steel interface at the outer edges of the bearing. This section of the model requires further mesh refinement to fully understand its character.

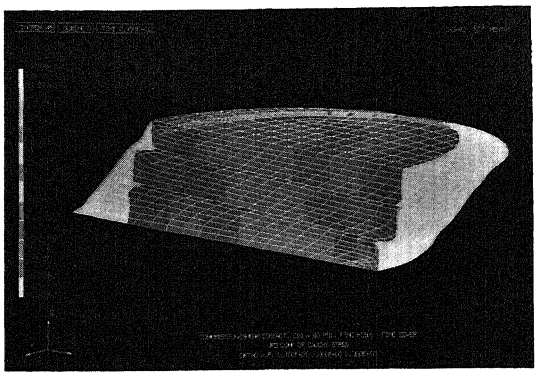

Figure 10. Z-component of Cauchy stress under 500 psi compression and equivalent 3D shear load of 10000 lbs.

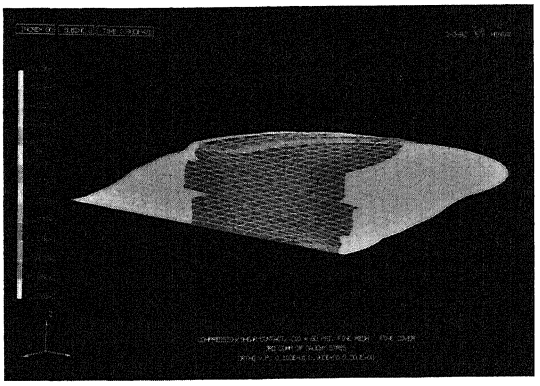

Figure 11. Z-component of Cauchy stress under 500 psi compression and equivalent 3D shear load of 18750 lbs.

The above bearing was also analyzed without cover rubber but with C_{10} = 65.3 psi, representing a slightly stiffer elastomer compound. The vertical displacement under 500 psi compression was 0.286 inches which was 13% larger than the experimental result. The addition of cover rubber gave a more accurate solution as long as enough elements were present in the cover rubber. Three elements in plan through the thickness of the cover rubber was the minimum necessary to achieve a stable result. The horizontal displacement at 10000 lbs shear loading without cover rubber was 4.4 inches , which was 14% larger than the experimental result.

2.3 *Comparison with 2D analysis*

Prior to the above analysis, two dimensional analysis were conducted on the same bearing using 8-noded plane strain elements. The 2D results for the bearing without cover rubber in compression were twice as stiff as the experimental results. Changing from a two-dimensional to a three-dimensional analysis effectively alters the shape factor of the modeled bearing to the true value. The actual bearing's shape factor was 2.25 as was the 3D FEM model's shape factor. However the two-dimensional model's shape factor was 4.5, twice the actual shape factor. Clearly, future two-dimensional analyses require an equivalent model that has the true 3D shape factor.

The effect of mesh refinement on the maximum shear strain at the steel rubber interface was explored using MARC Analysis Research Corporation's Adaptive Mesh technique. The mesh was adjusted so that it was very fine at the steel-rubber interface, yet coarse elsewhere. The maximum shear strain value improved to within 1% of the value given by use of equation (8) above.

3 CONCLUSION

As a result of the investigation reported on the mechanics of laminated isolation bearings, the distribution of stress in the steel shims, the bearing's axial stiffness, especially when combined with shear loads, the horizontal stiffness, and the effect of cover rubber on stiffness are becoming more clearly understood. From the results obtained it can be concluded that valid 2D analyses are difficult to achieve unless the shape factor is truly represented.

The inclusion of cover rubber is necessary if good correlation between experimental and theoretical displacements is to be achieved. In general the stiffness response of the bearing is not very sensitive to the mesh coarseness providing that the cover rubber is adequately represented, however the fineness of the mesh in local regions where the stress concentrations are high can significantly affect the accuracy of the solution in those regions.

Future investigations will address the problems of predicting the onset of roll-out and determining how boundary conditions represented by the top and bottom plates being connected by bolts or dowels influences the stress distribution. It is planned to further address these possibilities and examine higher shape factor bearings.

4 ACKNOWLEDGEMENTS

The continued interest and assistance of Ian G. Buckle and Helen Liu of the National Center for Earthquake Engineering Research and of Alan Muir and Hamid Ahmadi of the Malaysian Rubber Producer's Research Association is recorded with gratitude. This research was supported in part by the University of California, Irvine through an allocation of computer resources.

REFERENCES

Aiken, I., Kelly, J. and Tajirian, F. 1989. Mechanics of low shape factor elastomeric seismic isolation bearings. Report No. UCB/EERC-89/13. University of California, Berkeley.

Buckle, I. and Mayes, R. 1990. Seismic isolation: history, application and performance. *Earthquake Spectra* 6, 2,: 161-201.

Herrmann, L., et al. 1988. Nonlinear behavior of elastomeric bearings -- F.E. analysis and verification. *Journal of Engineering Mechanics*. ASCE 114, 11: 1831-1847.

James, A., Green, A. and Simpson, G. 1975. *Journal of Applied Polymeric Science* 19: 2033.

Kelly, J. Aiken, I. and Tajirian, F. 1990. Mechanics of high shape factor elastomeric seismic isolation bearings. Report UCB/EERC 90-01. University of California, Berkeley.

Stanton, J. and Roeder, C. 1982. Elastomeric bearings design, construction, and materials. National Cooperative Highway Research Program (NCHRP) Report No. 248. Washington, D.C.: Transportation Research Board.

Tajirian, F., Aiken, I. and Kelly, J. 1990. Seismic isolation for advanced nuclear power stations. *Earthquake Spectra*. Special Vol. 6, 2. California Earthquake Engineering Research Institute, El Cerrito.

Treloar, L. 1975. The physics of rubber elasticity. Oxford: Clarendon Press, 3rd edition.

Yeoh, O. 1990. Characterization of elastic properties of carbon-black-filled rubber vulcanizates. Presented at a meeting of the Rubber Division, American Chemical Society, Las Vegas Nevada.